Express Polymer Letters Vol.17, No.4 (2023) 417–433
Available online at www.expresspolymlett.com
https://doi.org/10.3144/expresspolymlett.2023.30

Research article

The influence of silicon-doped hydroxyapatite nanoparticles on the properties of novel bionanocomposites based on poly(3-hydroxybutyrate-*co*-3-hydroxyvalerate)

Mualla Öner[1*], *Semra Kirboga*[1], *Emrah Şefik Abamor*[2], *Kubra Karadaş*[2], *Zeynep Kral*[1]

[1]Yıldız Technical University, Department of Chemical Engineering, Davutpasa Campus, 34210 Esenler, İstanbul Turkey
[2]Yıldız Technical University, Department of Bioengineering, Davutpasa Campus, 34210 Esenler, İstanbul, Turkey

Received 9 August 2022; accepted in revised form 14 November 2022

Abstract. In this study, silicon-doped hydroxyapatite (SiHAP) nanoparticles and poly(hydroxybutyrate-*co*-3-hydroxyvalerate, PHBV) were used to develop biodegradable 'green' composites due to their intrinsic biodegradability and biocompatibility properties. The novel bionanocomposites were prepared by melt compounding with 0.5, 2, and 3 wt% of SiHAP content. The fracture surface of the bionanocomposites samples from scanning electron microscopy (SEM) exhibited good dispersion of SiHAP in the PHBV matrix at 0.5 wt%. X-ray diffraction (XRD) measurements showed an enhancement of the crystallinity of the PHBV matrix, thereby acting as a nucleating agent, increasing polymer crystallinity from 50 to up to 73% at 3 wt% loadings. Dynamic mechanical analysis (DMA) was used to measure the composite and neat samples' storage modulus, loss modulus, and damping factor under an oscillating load. DMA analysis showed an increase in storage modulus of 80% at 20 °C and 0.5 wt% SiHAP loadings. Thermal gravimetric analysis (TGA) results showed that the thermal stability of PHBV is slightly decreased by adding 2 and 3 wt% SiHAP. 3-(4,5-dimethylthiazol-2-yl)-2,5-diphenyltetrazolium bromide (MTT) Assay and 4′,6-diamidine-2′-phenylindole dihydrochloride (DAPI) staining experiments have demonstrated that PHBV/SiHAP composites exhibit good *in vitro* bioactivity due to the silicon-doped hydroxyapatite nanoparticles. It is concluded that the addition of SiHAP can be a viable strategy for obtaining novel bioactive and biodegradable nanocomposites with improved mechanical and biological properties for potential medical application.

Keywords: *biopolymers, biocomposites, biocompatible polymers, biodegradable polymers, reinforcements, mechanical properties*

1. Introduction

Biodegradable polymers, which are harmless to the environment, have attracted the attention of many researchers. They are increasingly used in all fields of medicine, especially in applications where biodegradability provides an advantage for the human body. The most widely studied and well-known biodegradable polymers are polyhydroxyalkanoates (PHAs), Poly(lactic acid) PLA, and starch [1–3]. PHAs are a big family of biodegradable and biocompatible microbial biopolyesters from renewable resources [4]. The first PHA identified by the French bacteriologist Maurice Lemoigne in 1926 was polyhydroxybutyrate (PHB) [5]. The most important features of PHB are its biocompatibility in all environments and its biodegradability. A standard component of human blood is 3-hydroxybutyric acid (3HB), and PHB decomposes into 3HB [6–8]. This proves that the PHB is highly biocompatible and non-toxic. Recently, the number of *in vivo* and *in vitro* studies on PHB has increased. It was shown that by increasing calcium flow in cultured cells, 3HB molecules suppress cell death and prevent serum withdrawal-induced apoptosis [8]. PHB-based biomaterials are

*Corresponding author, e-mail: muallaoner@gmail.com

piezoelectric that can improve bone growth *in vivo* [8]. It has been observed that PHB is compatible with cells such as epithelium, osteoblast, bone tissue, and blood [9]. Some applications of PHB in biomedical and tissue engineering are drug delivery systems, cardiovascular devices, heart valves, and nerve cuffs, but the difficulty of processing PHB limits its application. To overcome its disadvantages, PHB copolymers can be synthesized with other hydroxyalkanoate monomers, mixtures containing another biopolymer can be prepared, or a PHB-based block can be synthesized. Poly(3-hydroxybutyrate-*co*-3-hydroxyvalerate, PHBV) copolymer is synthesized by the incorporation of 3-hydroxyvalerate (3HV) monomer components of various molar ratios into the 3-hydroxybutyrate (3HB) polymer chain. Some of the shortcomings of PHB improve with the incorporation of 3HV. PHBV has lower melting temperature, stiffness, elasticity modulus, and higher impact strength than PHB [10]. Thus, studies on the poly(3-hydroxybutyrate-*co*-3-hydroxyvalerate) copolymer (PHBV) for biomedical applications have increased. PHBV is obtained by the copolymerization of hydroxybutyrate and hydroxyvalerate. PHBV consists of 0 to 24% hydroxyvalerate (HV) units and hydroxybutyrate (HB) units that appear randomly along the polymer chain. PHBV can promote bone growth *in vivo* due to its degradable, biocompatible, and piezoelectric properties [11, 12]. The properties such as biodegradability and biocompatibility are sufficient for use in PHBV cell culture [13]. It is known that the degradation time of PHBV is longer when compared to other biocompatible polymers [14, 15]. In studies in mice and rats, PHBV was found to be minimally inflammatory in long-term subcutaneous implant applications [15]. Studies show that PHBV is a promising polymer in long-term bone regeneration applications [14]. With the degradation of PHB and PHBV polymers, products that are standard components of human blood are formed, so they give less inflammatory response to the human body than other polymers [16]. The degradation rate of PHBV increases with increasing pH. Hydrolysis of PHBV is slow in the neutral medium at body temperature. At the same temperature and pH, the *in vitro* hydrolysis rate is lower than *in vivo* degradation rate of PHBV [14]. The degradation rates of PHBV and cell/PHBV structures capable of producing neo-cartilage in a heterotopic region continue to be investigated [17]. Therefore, using PHBV as a matrix phase in composite materials is significant potential.

The contribution of nanoscale ceramic fillers in biodegradable polymers to medical applications is undeniable, as they show excellent improvements in material properties, even in low amounts. The most similar ceramic fillers to the mineral part of the bone are hydroxyapatite ($Ca_{10}(PO_4)_6(OH)_2$), which exhibits high biocompatibility, bioactivity, osteoconductivity, and an affinity for biopolymers. Therefore, it can be used to repair hard tissues [18].

Synthetic hydroxyapatite (HAP) used in biomedical applications has poor toughness, a low *in vivo* degradation rate, and low mechanical strength. The fact that synthetic HAP has these disadvantages limits its applications. When human bone is examined, it has been observed to contain very few ionic additives such as Si^{4+}, F^{-}, and Sr^{2+} in its structure. Since ions such as Si and Sr are in natural bone tissues, they were considered dopants and were thought to benefit the biological response of osteoblasts [19, 20]. The main inorganic mineral of bones is hydroxyapatite, doped with various trace elements [19, 20]. The solubility, morphology, surface properties, and particle size of HAP are affected by ion doping in HAP. Ion dopants can also affect the biological activity of HAP. Silicon, which requires small amounts of Si, is found in many animal organs. In the case of Si deficiency, bone and joint diseases are observed. HAP doped with Si can be used in bone repair by improving the functionality of traditional biomaterials [19]. Studies on Si-doped HAP have shown that the crystallinity of Si-doped HAP and the amount of amorphous phase can be affected by high Si-doping content [19]. The expected properties of Si-doped HAP are that it is both biocompatible and has a bone formation-supporting effect [21]. In the literature, in studies with Si-doped HAP materials, cell adhesion and proliferation increase *in vitro* [22]. Si-doped HAP was found to be better biocompatible than undoped HAP when the growth of osteoblastic cells was evaluated [23]. *In vitro,* osteogenic-related gene expressions in human bone marrow cells can be up-regulated by Si-doped HAP [24]. Apatite formation was evaluated by applying Si-doped HAP to the simulated body fluid. Using Si-doped HAP, the appearance of the apatite layer on the surface was significantly improved [25].

PLA, PHB, and PHBV composites with hydroxyapatite have been studied by many researchers. PLA/HAP biocomposite recommended for medical applications has been considered a good alternative to produce bone graft substitutes. Hydroxyapatite, which

has properties close to the structure of bone, has been used to strengthen poly-1-lactic acid (PLA), which is used in many orthopedic applications [26, 27]. The study of Russias *et al.* [26] aimed to combine HAP's bioactivity and mechanical properties with the absorbability of PLA. As a result of the degradation of pure PLA implants in the body, the amount of intermediate acidic products that cause negative inflammatory responses could increase. The addition of HAP may help as a solution to this problem. *in vitro* degradation in body fluid was investigated with PLA/HAP composite by simulating the factors controlling the final properties [26]. It has been found that PHB/HAP composites can be used for rapid bone healing and new bone formation [28]. The biocompatibility of the nanocomposite of PHB with hydroxyapatite is an important area of study [9]. Differentiation was observed in PHB composites with the change in the amount of hydroxyapatite in the composite [29]. The efficiency of a biomaterial depends on the additive's ability to interact with cells, but there is not much data on interaction for the PHB/HAP nanocomposite [30]. In the study of Yuan *et al.* [31], nanoscale hydroxyapatite was incorporated into poly(hydroxybutyrate-*co*-3-hydroxyvalerate) (PHBV) polymer, and a composite was obtained by solvent casting method. Homogeneous dispersion of HAP nanoparticles on the composite films and good bonding to the polymer was achieved. It has been observed that the ability to adsorb human fibrinogen can be improved with the obtained composite. PHBV/ HAP composites were prepared by solvent casting [32]. The material bioactivity increased, and higher glass transition was obtained due to the reinforcement effect of HAP. PHBV/HAP films were produced by surface-treated HAP [33]. The results showed that surface treatment led to higher tensile force. Sadat-Shojai *et al.* [8] prepared PHB/HAP composite by solution casting method. It was observed that HAP strongly affects cell growth and proliferation, enhancing metabolic activity. Öner and İlhan [34] prepared PHBV/HAP composite using the melt extrusion method. The highest tensile properties were obtained for 5 wt% surface-treated HAP loading.

This research aimed to develop and characterize a novel biocomposite using polyhydroxybutyrate-*co*-valerate (PHBV) and Si-doped HAP for potential medical applications. To the best of our knowledge, the effect of Si-doped HAP on the properties of PHBV composite has not yet been reported. The biocomposites were prepared using melt extrusion. The composites' physical, thermal, dynamic mechanical, and bioactivity were characterized as a function of the Si-doped loading. This study demonstrates that preparing PHBV composites with Si-doped HAP significantly promotes dynamic mechanical properties and bioactivity.

2. Experimental

2.1. Materials

Under the brand name MAJ'ECO FN000HA, poly(3-hydroxybutyrate-*co*-3-hydroxyvalerate, or PHBV), with an 8 mol% hydroxyvalerate content, was obtained from ADmajoris Company, France. Hydroxyapatite (HAP) doped with 5% of silicon (SiHAP) was purchased from Sigma-Aldrich Chemicals (St. Louis, USA) (surface area 10–15 m^2/g; particle size <200 nm). The human osteoblastic osteosarcoma (SaOs-2) cell line was purchased from American Type Culture Collection (ATCC). 3-(4,5-dimethylthiazol-2-yl)-2,5-diphenyltetrazolium bromide (MTT) and 4′,6-diamidine-2′-phenylindole dihydrochloride (DAPI) were purchased from Sigma-Aldrich Chemicals (St. Louis, USA). Dulbecco's modified eagle's medium and Fetal Bovine Serum were purchased from Gibco Life Technologies (Paisley, UK). Penicillin/streptomycin was purchased from Capricorn Scientific (Ebsdorfergrund, Germany).

2.2. Composite preparation

In this work, an extruder was used to prepare PHBV/SiHAP composites. All materials used were dried at 50 °C in a vacuum oven before use. The desired concentrations of SiHAP were added to PHBV in a twin-screw extruder (Rondol Microlab England; *L*/*D*: 20). From the feed section to the endpoint, the extruder applied temperatures at 90–135–160–160–150 °C while operating at a screw speed of 80 ppm. Unfilled PHBV was also melt-processed under the same conditions to prepare a reference material. The PHBV nanocomposites films were then compression molded into 0.75 mm thick with a hot-cold press machine (Gülnar Makine, Turkey). The obtained composite samples were coded as PHBV-SiHAPX. The number X in the sample represents the percent by weight of SiHAP in the composite. Example, sample PHBV-SiHAP0.5 shows the sample obtained in the presence of 0.5% SiHAP.

2.3. Scanning electron microscopy

Scanning electron microscopy (SEM) was performed using an FEI-Philips XL 30 ESEM-FEG (Thermo Fisher Scientific, Nederlands) scanning electron microscope at an accelerating voltage of 5 kV. Composite samples that had been cryogenically broken were attached to typical SEM stubs and were coated in gold to reduce the sample's charge inside the instrument.

2.4. X-ray diffaraction pattern

X-ray diffraction (XRD) measurement with Cu K_α source ($\lambda = 0.15418$ nm) was performed at 40 kV and 20 mA using the X'Pert Pro (Philips diffractometer, PANalytical, Denver, Colorado) device. The patterns were recorded for a 2θ range from 4 to 80°. The Scherrer equation is used to determine the crystal size.

2.5. Thermal analysis

A Perkin Elmer TGA analyzer (USA) was used to perform thermogravimetric analysis (TGA) measurements on samples weighing around 10 mg. Each sample was heated at a rate of 10 °C/min under nitrogen at a flow rate of 10 ml/min as the temperature ranged from ambient to 600 °C.

2.6. Fourier transformation infrared spectroscopy

To compare the variation in the functional group of the neat PHBV and its composites, a Bruker ALPHA-P Fourier transformation infrared spectroscope (FTIR, Bruker, Toronto, Canada) was used in transmittance mode at wavelengths ranging from 500 to 4000 cm^{-1}.

2.7. Dynamic mechanical analysis of samples

Dynamic mechanical analysis (DMA) was performed using the Perkin-Elmer DMA8000 (PerkinElmer, USA). The dynamic characteristics of samples were examined in single cantilever mode at 1 Hz using film extension mode in the temperature range of –30 to 150 °C at a heating rate of 2 °C/min. The test samples were 10.40 mm × 10 mm in size. The testing involved determining and recording the storage modulus E', loss modulus E'', and $\tan\delta = E''/E'$ values *vs*. temperature.

2.8. Cell cultivation

Human osteoblastic osteosarcoma (SaOs-2) cells were cultivated in Dulbecco's modified Eagle's medium (DMEM) supplemented with 10% fetal bovine serum (FBS) and 1% penicillin/streptomycin at 37 °C in an incubator enriched by 5% CO_2. The culture medium was refreshed every two days.

2.9. Scaffold sterilization and preparation for cell culture

Before use in cell culture studies, scaffolds were cut into several squares with dimensions of 5 mm × 5 mm. For sterilization, scaffold pieces were treated with 70% ethanol solution for 30 minutes. After that, scaffold pieces were irradiated with UV light overnight. After sterilization, scaffolds were transferred into test tubes containing 3 ml DMEM medium supplemented with 10% FBS. Then test tubes were incubated at 37 °C for 48 hours. Due to the scope of the extraction method, medium supernatants were collected and used for further cytotoxicity investigation.

2.10. MTT assay

To measure cell viability rates of osteoblast cells after treatment with scaffold extracts, 3-(4,5-dimethylthiazol-2-yl)-2,5-diphenyltetrazolium bromide (MTT assay) was used. Briefly, $1 \cdot 10^4$ osteoblast cells with a final volume of 100 µl were transferred into each well of the 96 well microplate and incubated at 37 °C overnight. After incubation, 10 µl of scaffold extracts were included in each well. The wells that were not exposed to extracts were used as the control. After that, microplates were incubated at 37 °C for 96 hours. After incubation, 10 µl of MTT solution (10 mg/ml) dissolved in phosphate buffer solution (PBS) was added to each well of the microplates. Then microplates were left to incubate for 4 hours. Afterward, formazan crystals in each well were dissolved with the addition of 100 µl dimethyl sulfoxide (DMSO). Then plates were left to incubate at room temperature in the dark. Finally, the absorbance of each well was read in an ELISA reader at 570 nm. By comparison of absorbance values in control and test groups, cell viability ratios were evaluated following exposure to tissue scaffolds.

2.11. DAPI staining

To determine the biocompatibility of scaffolds, the DAPI staining method was used. For that purpose, sterilized scaffolds were inserted into each well of the 24 well plate and seeded with $1 \cdot 10^4$ osteoblast cells. For a week, the plates were incubated at 37 °C. Every two days, the medium was renewed. Cells

were fixed with 4% paraformaldehyde for 10 minutes after incubation, and they were then washed with PBS. Finally, cells and scaffolds were exposed to DAPI stain for 20 minutes. After exposure, cell-seeded scaffolds were washed with PBS twice, and cell attachment was considered by using a fluorescent microscope.

3. Results and discussion

3.1. Morphological characterization of particles and composites

To assess the morphology of SiHAP particles, scanning electron microscopy (SEM) was used, and their micrograph is presented in Figure 1. Through SEM investigation of 210 particles, the distribution of spherical dimensions was determined (Figure 1b). Each distribution curve was fitted using a Gaussian distribution function. The distribution curve appears to have two peaks in the SEM results for these crystals, which demonstrate two size ranges. (Figure 1b). As observed in the particle histogram, most of the uniform spherical SiHAP nanoparticles presented diameter sizes between 35 and 75 nm, with an average diameter of 55 nm. The average diameter of the particles in the second peak, which has a large particle distribution, is about 470 nm.

The melt-processing method was used to prepare PHBV/SiHAP composites. This method does not involve solvent in the process. So, it is greener compared to the solvent casting method. The morphology of the cryo-fractured surface of PHBV and respective composites was examined by scanning electron microscopy (SEM) to investigate the dispersion of the SiHAP particles in the polymer matrix. Figure 2 illustrates the composites at 10 000× magnification. SEM pictures reveal spherical nanoparticles randomly and well distributed within the PHBV matrix at 0.5% SiHAP loadings. However, it can be observed that as the nanofillers content increases, the SiHAP nanoparticle dispersion is poorer and has a higher tendency toward aggregation. Therefore, the samples containing 2 and 3 wt% loading (Figures 2b and 2c) showed a biopolymer matrix with filler aggregates of SiHAP. The morphological examination reveals that low concentrations of HAP in PHBV disperse as single particles, but both single particles and tiny clusters appear at greater loadings. This could result from the filler-matrix interface having high surface tension, which results in poor interactions between the polymer and SiHAP particles. Another explanation might be that the extrusion procedure failed to sufficiently break down the HAP aggregate during melt compounding.

3.2. XRD results

In Figure 3a, the XRD pattern shows crystallographic structures of Si-doped HAP particles. Compared to the JCPDS 98-028-9993 standards, each peak of the patterns in Figure 3a corresponds to the hydroxyapatite phase. It has a hexagonal crystal system. The unit cell dimensions are $a = 9.4330$ Å, $b = 9.4330$ Å, and $c = 6.8960$ Å, respectively. There are no additional peaks in the Si-doped HAP patterns compared to the peaks of standard HAP. The silicon-doped HAP samples were prepared using the hydrothermal method [19]. They found that Si doping did not produce a new phase apart from the hydroxyapatite phase. In this work, the characteristic peaks appear at 22.6, 25.6, 30.4, 32.7, 33.6, 39.7, 46.2, 49.1, and 52.8°, corresponding to diffraction planes including (111), (002), (211), (300), (202), (310), (222), (213) and (004) of hydroxyapatite. Three planes (211), (300), and (202) are significant peaks of HAP.

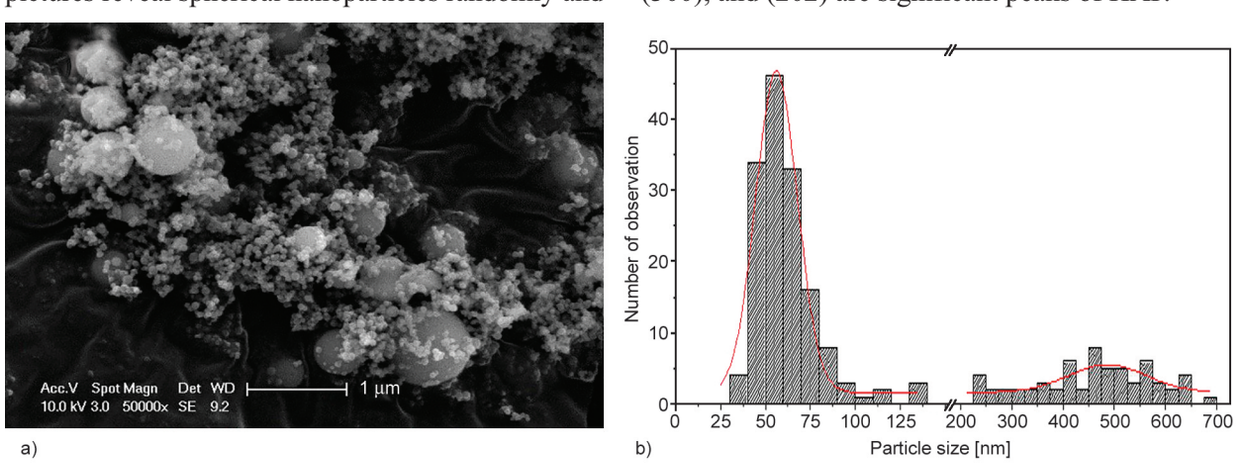

Figure 1. SEM photograph of a) SiHAP and b) particle size distribution of SiHAP.

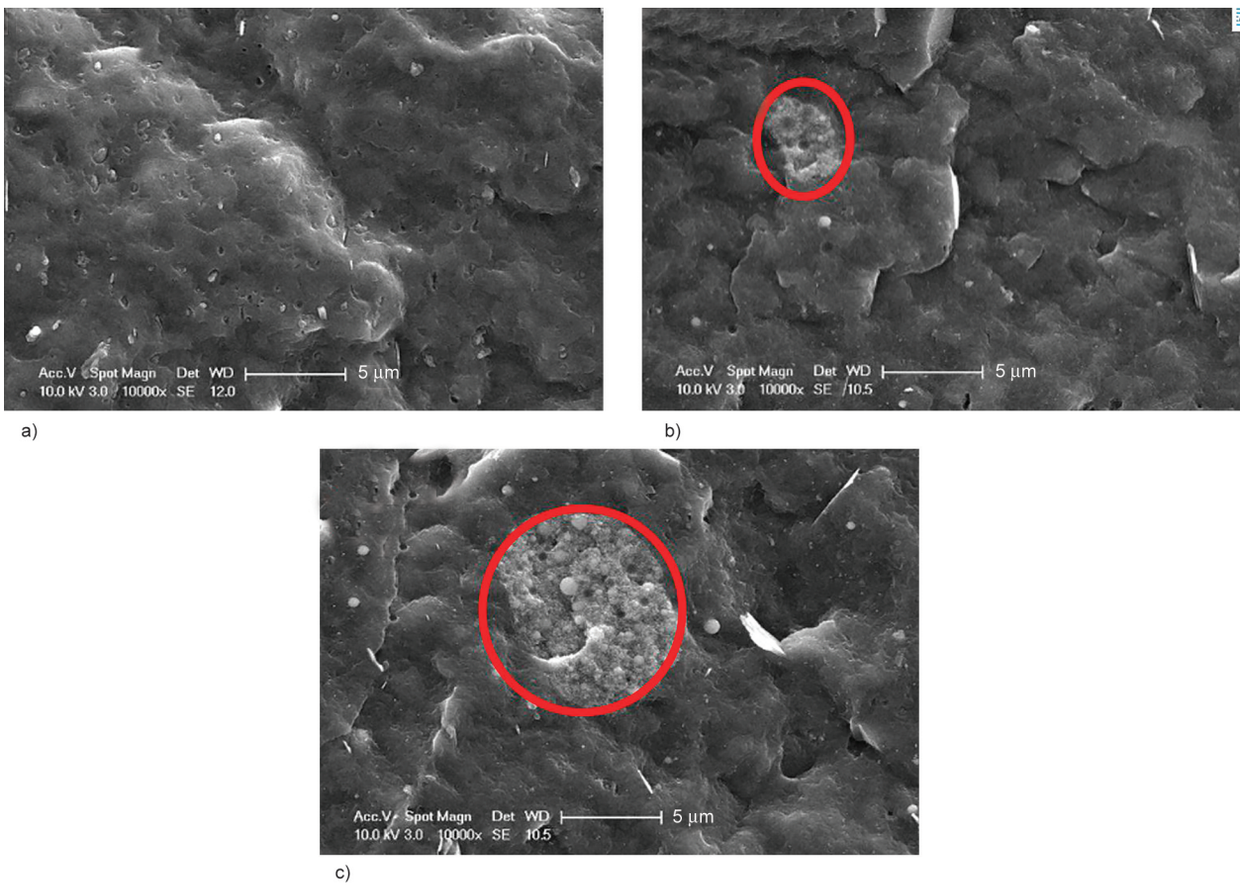

Figure 2. SEM photograph of composites a) PHBV-SiHAP0.5, b) PHBV-SiHAP2.0 and c) PHBV-SiHAP3.0.

Figure 3b displays the XRD spectra of the composites and neat PHBV. Neat PHBV characteristic peaks at 2θ = 13.3, 16.7, 19.9, 21.2, 25.4, 26.7, and 29.8° correspond to (020), (110), (021), (101), (121), (040) and (002) planes with an orthorhombic lattice [35, 36]. The structure of the polymer corresponds to the usual α-form described for P3HB [37]. The same characteristic reflections of the PHBV, which provide detailed information about its crystal structure, were observed after incorporating SiHAP. This result indicates that the particles did not alter the crystalline structure of the polymer. However, after the addition of SiHAP, the intensity of the PHBV peaks becomes stronger and sharper when compared to the neat PHBV matrix, even in the form of agglomerates at higher concentrations, attributed to SiHAP incorporation, which acts as a nucleating agent tends to increase the ordering level of PHBV molecular chains and to facilitate the crystallization of PHBV, as observed by other researchers.

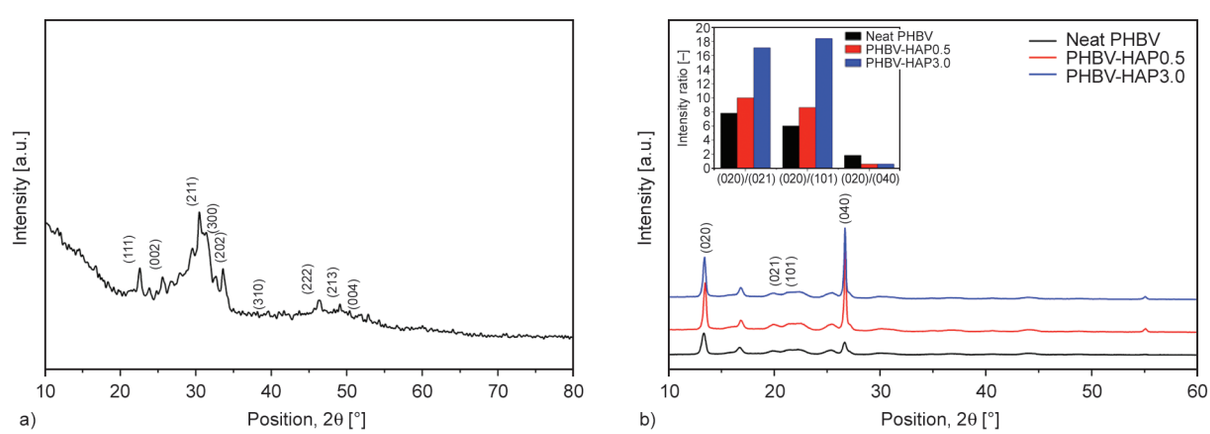

Figure 3. The X-ray diffraction pattern of the a) SiHAP and b) PHBV-SiHAP composites.

In previous studies, PHBV composites using bacterial cellulose [38], boron nitride particles [39], and nanocellulose fillers [40] have all shown a similar effect.

This difference can be explained by analyzing the intensity ratio of the planes (020)/(021), (020)/(101), and (020)/(040) (Table 1). For (020)/(021) planes, the relative intensity ratio of the neat PHBV was 8.56, but for PHBV-SiHAP0.5 and PHBV-SiHAP3 nanocomposites, it was 10.00 and 17.09, respectively. The increase in the relative ratio suggests that the presence of SiHAP particles enhanced crystal formation in the (020) crystal plane. This phenomenon was previously observed by other researchers for PHBV-graphene nanocomposites [41], PHBV-functionalized cellulose nanocrystal composites [42], and PHBV-Boron nitride composites [39]. On the other hand, the intensity ratio of the (020)/(040) decreases from 1.82 to 0.57 for neat PHBV and PHBV-SiHAP3, respectively. The decrease in the (020/040) relative ratio suggests that, despite an increase in both peak intensities due to the addition of SiHAP, the peak intensity of the (040) peak increases more than the intensity of the (020) peak.

The incorporation of SiHAP produced sharper peaks for the (020), (021), and (101) PHBV reflections compared to neat PHBV. The crystallite size dimension L_{020} [nm] was determined using the Scherrer formula for the direction normal to the *hkl* plane (Equation (1)):

$$L_{(020)} = \frac{k\lambda}{B\cos\theta} \tag{1}$$

where $L_{(020)}$ indicates the average crystallite size in nanometers, k for the shape constant, and B for the diffraction line's broadening as measured at 50% of its highest intensity. B is the diffraction peak under consideration's full width at half maximum intensity (FWHM). When FWHM is utilized for B, the shape factor k becomes 0.9. λ is the X-ray wavelength, and θ is the Bragg diffraction angle.

Table 1 shows the effect of SiHAP on the crystalline lamellae size for the (020) reflection and the crystallinity index. The Equation (2) was used to obtain the crystallinity index (CI [%]) values for samples based on XRD measurements [43, 44]:

$$CI_{(020)}[\%] = \frac{I_{(020)}}{I_{\text{Total}}} \cdot 100 \tag{2}$$

where $I_{(020)}$ is the intensity of the diffraction peak of the (020) plane, peak at 2θ = 13.3°, and I_{Total} is the total intensity value of all crystalline peaks of PHBV. The crystallite size L [nm] calculated for the (020) reflection peak and crystallinity index value was 20.32 nm and 44.70% for neat PHBV, respectively. Addition of SiHAP, both crystallinity and crystal dimensions were increased significantly and varied with SiHAP content. The composites showed higher crystallinity and crystal sizes. The crystallite size and crystallinity values were 35.19 nm and 71.87% for PHBV-SiHAP3 nanocomposites, respectively.

3.3. FTIR results

FTIR spectra of the SiHAP crystals and neat PHBV is given in Figure 4a. In the SiHAP spectrum, the bands at 560 cm^{-1} represent the O–P–O bending mode, and the band at 1036 cm^{-1} corresponds to P–O stretching vibration. No additional peaks were observed for Si-doped HAP. The exhibited peaks also coincide with the structure of HAP, which supports the XRD patterns.

The FTIR transmittance (T) spectra of composites are given in Figure 4b. PHBV composites exhibit the same characteristics peak of neat PHBV. The absorption peaks at around 2977, 2928, and 2859 cm^{-1} could be assigned to $–CH_3$ asymmetric stretching, $–CH_2$ antisymmetric stretching, and $–CH_3$ symmetric stretching, respectively. The FTIR spectrum showed the characteristic peaks at 1711 cm^{-1} (carbonyl group) and 1170 cm^{-1} (C–O–C antisymmetric stretching). The peak is observed at 1711 cm^{-1} due to the C=O stretching vibration in the ester group of PHBV. The peak around 1460 cm^{-1} indicates CH_2 scissoring. The peaks at 1268 and 1170 cm^{-1} may be assigned to C–O–C stretching vibration. The peak in the range of 821–972 cm^{-1} could be assigned to C–O–C symmetric stretching. CH_2 wagging may be observed in

Table 1. Values of $L_{(020)}$ [nm], intensity ratios, and CI [%] of composites obtained from the XRD scan.

Sample	$L_{(020)}$ [nm]	(020)/(021) 13.3/19.8	(020)/(101) 13.3/21.2	(020)/(040) 13.3/26.6	$CI_{(020)}$ [%]
Neat PHBV	20.32	8.56	6.01	1.82	44.70
PHBV-SiHAP0.5	30.79	10.00	8.62	0.60	59.45
PHBV-SiHAP3.0	35.19	17.09	18.41	0.57	71.87

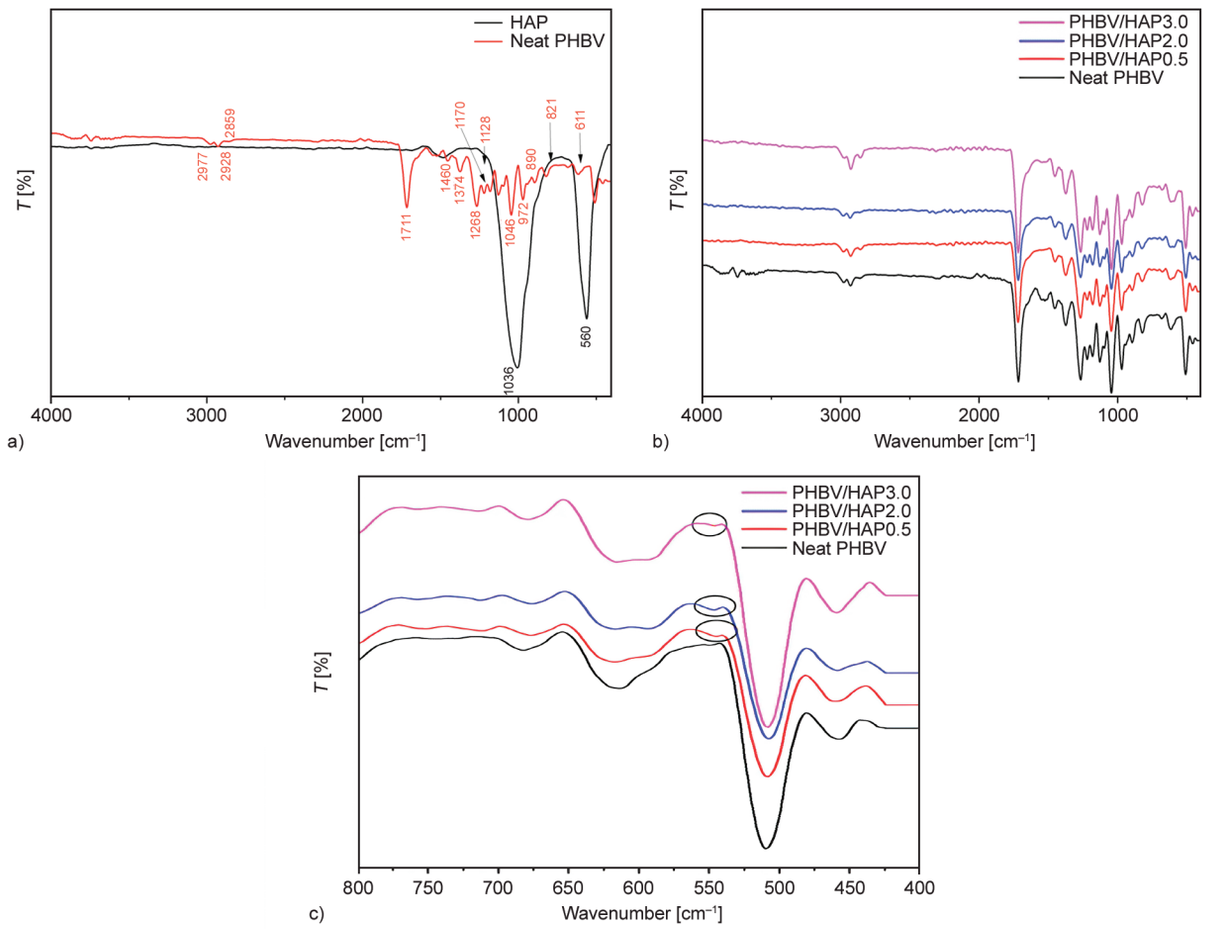

Figure 4. FTIR spectrum of a) SiHAP and neat PHBV at 400–4000 cm^{-1}, b) PHBV-SiHAP composites, and c) PHBV-SiHAP composites at 800–400 cm^{-1}.

the field of 1128–1374 cm^{-1}. Some of the characteristic absorption peaks of SiHAP and the PHBV in the composites overlap. Therefore, it was challenging to demonstrate the distinct differences between PHBV and PHBV-SiHAP composites by FTIR studies. SiHAP has a strong absorption band at 560 cm^{-1} due to the bending vibration of O–P–O bond (Figure 4a). This band is also present at roughly the same location in the spectra of PHBV-SiHAP nanocomposites, and the intensity of the peak increases with the SiHAP content of the composites (Figure 4c). This result validated the inclusion of SiHAP nanoparticles in the PHBV matrix.

3.4. TGA results

Thermogravimetric analyses (TGA) were carried out to evaluate the effect of the addition of the SiHAP on the thermal stability of PHBV nanocomposites. The thermal degradation (TG) and derivative thermogravimetric (DTA) curves of the neat polymer and composites are shown in Figures 5, and representing temperature is given in Table 2. TGA thermograms show that neat PHBV and composites present one single decomposition step profile. The decomposition step occurs fast, starting at 271.1 °C for neat polymer, and completes at 297.5 °C. The key findings are summarized in Table 2 as the initial degradation temperature (T_i), the degradation temperature T_{10} corresponding to a mass loss of 10 wt%, the mid-point of degradation (T_{50}) recorded at a mass loss of 50 wt%, and the maximum loss temperature (T_{max}).

The initial (T_i) degradation temperatures of the PHBV have not been affected by the addition of 0.5 wt% SiHAP. However, the addition of 2 and 3 wt% SiHAP gently moves the peak of the TGA curves to the left, indicating that the addition of SiHAP in this concentration decreases the thermal stability of PHBV. Figure 5b shows the DTA curve, and the peak represents the temperature corresponding to the maximum degradation rate (DTA_{peak}). For neat PHBV, DTA_{max} occurred at 287.9 °C. However, the addition of SiHAP shifted the DTA_{max} to a lower temperature. The DTA_{max} for PHBV-SiHAP3 occurred at 274.2, which is 13.7 °C lower than the neat PHBV.

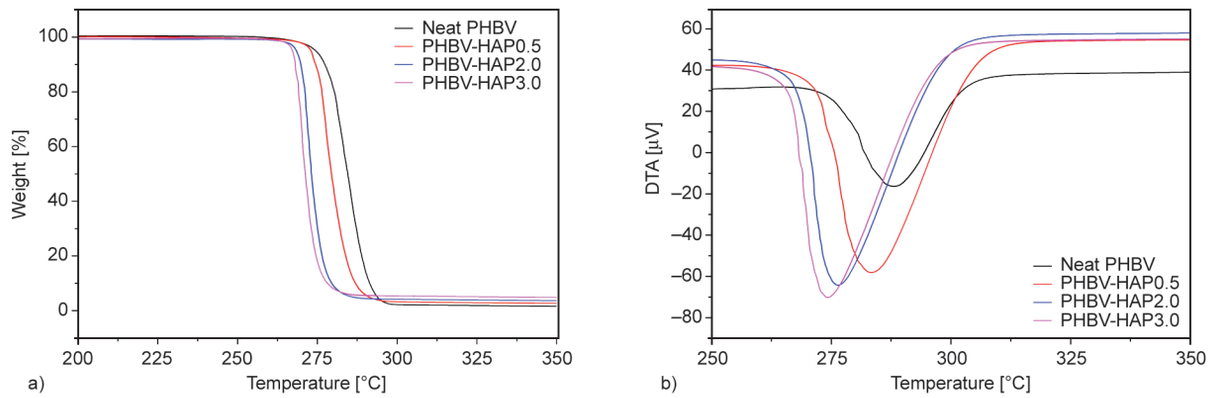

Figure 5. a) TGA and b) DTA curves of neat PHBV and PHBV-SiHAP nano biocomposites.

Table 2. TGA values of PHBV-SiHAP biocomposites.

Sample code	T_i [°C]	T_{10} [°C]	T_{50} [°C]	T_{90} [°C]	T_{max} [°C]	DTA_{peak} [°C]
Neat PHBV	271.14	277.29	284.56	291.28	297.53	287.90
PHBV-HAP0.5	270.37	274.43	279.44	286.82	294.93	283.60
PHBV -HAP2.0	266.28	269.81	273.17	279.25	286.58	276.20
PHBV -HAP3.0	265.24	268.07	271.21	278.04	283.76	274.20

The reduction of T_i and T_{max} values for PHBV was previously reported in the literature for incorporation of lignosulfonate [45], cellulose nanowhiskers [46], lignin [47], nanohydroxyapatite (nHAP) and diamond nanoparticles [48] and graphene nanosheets [41, 49]. The possible reason for this effect was reported as the high thermal conductivity of the particles, which enhanced the heat diffusion throughout the material. Castro-Mayorga *et al.* [50] synthesized ZnO particles by an aqueous precipitation method. They used different methods to fabricate PHBV/ZnO nanocomposites, including melt-mixing and electrospinning. T_{max} value of PHBV was decreased by ZnO particle addition, reducing the thermal stability. This effect was attributed to ZnO's high thermal conductivity and catalytic properties. Chen *et al.* [32] fabricated the PHBV/HAP nanocomposite using the solution casting method with strong ultrasonication. The incorporation of nHAP resulted in the decomposition of the polymer matrix at the initial stage. T_i value for PHBV/ HAP (100/50) dropped by 5 °C compared to that for the pure polymer. The composites of polylactide (PLA) or poly(3-hydroxybutyrate-*co*-3-hydroxyvalerate) (PHBV) were prepared by extrusion and injection molding using ZnO nanoparticles [51]. The results showed that the onset and peak degradation temperature of PLA was shifted towards lower temperatures with the increase of ZnO concentration, while degradation of PHBV showed no dependence on the ZnO concentration [51]. Braga *et al.* [52] prepared PHBV-TiO_2 composites by using the electrospinning technique, to be used as a scaffold. The decrease in the thermal degradation temperature was observed in the presence of the nanoparticles. This observation was explained due to the presence of agglomerations of the nanocomposites in the fiber; the interactions of the PHBV with TiO_2 were reduced and affected the random chain scission reaction of PHBV during the thermal degradation process [52]. The same argument can be considered in this work since SiHAP particles tend to agglomerate, especially at high concentrations. The aggregation of SiHAP reduced the bonding interactions between PHBV and nanoparticles, thus weakening the thermal stability.

3.5. Dynamic mechanical analysis (DMA) of composites

The mechanical properties of a polymer are strongly influenced by temperature, which affects a decrease in the material's rigidity and an increase in its viscous flow. These variations are reflected in the storage modulus, loss modulus, and loss factor. All samples exhibited a typical behavior of semi-crystalline polymer with a decrease in storage modulus by an increasing temperature. The decline in storage modulus with temperature is due to the increased molecular motion of the matrix molecules. As the temperature rises, the lattice polymer chains can move more freely, reducing the considerable stress within

the polymeric framework resulting in a decrease in modulus.

The storage modulus values against the temperature of PHBV composites are shown in Figure 6a compared to neat PHBV. According to the dynamic mechanical analysis (DMA) results, SiHAP nanocrystals affect the storage modulus of the PHBV overall temperature ranges, as shown in Figure 6a. The strongest reinforcing effect was observed for composites of 0.5 wt% of SiHAP. Figure 6a shows that at –20 °C, the E' of PHBV/SiHAP0.5 is 7.4 GPa as opposed to neat PHBV with an E' of 3.9 GPa. For comparison, four temperature settings were used: –20 °C as an indicator of the glassy behavior, 20 °C for room temperature behavior, 37 °C for body temperature behavior, and 80 °C as an indicator of the high-temperature behavior of the composite. At –20 °C, the highest relative storage modulus increases were obtained compared to the neat PHBV, corresponding to 86, 64, and 42% for 0.5, 2, and 3 wt% SiHAP contents, respectively. The storage modulus of neat PHBV increases by 80% for PHBV-SiHAP0.5 at 20 °C. At 37 °C, the E' of PHBV increased by 69% for PHBV-SiHAP0.5. On the other hand, a 67% increase in the storage modulus of PHBV is observed for the sample containing 0.5 wt% SiHAP at 80 °C. The storage modulus measures a material's capability to store mechanical energy without dissipating it and to withstand deformation. PHBV composites are more resistant to deformation and, therefore, more rigid than neat polymers. This mechanical reinforcement effect was attributed mainly to the high stiffness and the good affinity through interfacial interaction between the biopolymeric matrix and SiHAP.

The loss modulus, E'', values of the PHBV and composites as a function of temperature at 1 Hz are presented in Figure 6b. The variation's trend was similar to the E' for loss modulus. This study observed that the loss modulus of neat PHBV was lower than the moduli of all composites, indicating that SiHAP improves the composite materials' damping and internal friction properties. Figure 6b shows the increase in loss modulus as the temperature rises from –30 °C to T_g due to molecular friction. The maximum increase was observed with PHBV-SiHAP0.5 followed by PHBV-SiHAP2 and PHBV-SiHAP3. Increased filler loading improved the PHBV composites' capacity to dissipate energy, as indicated by the increase in the

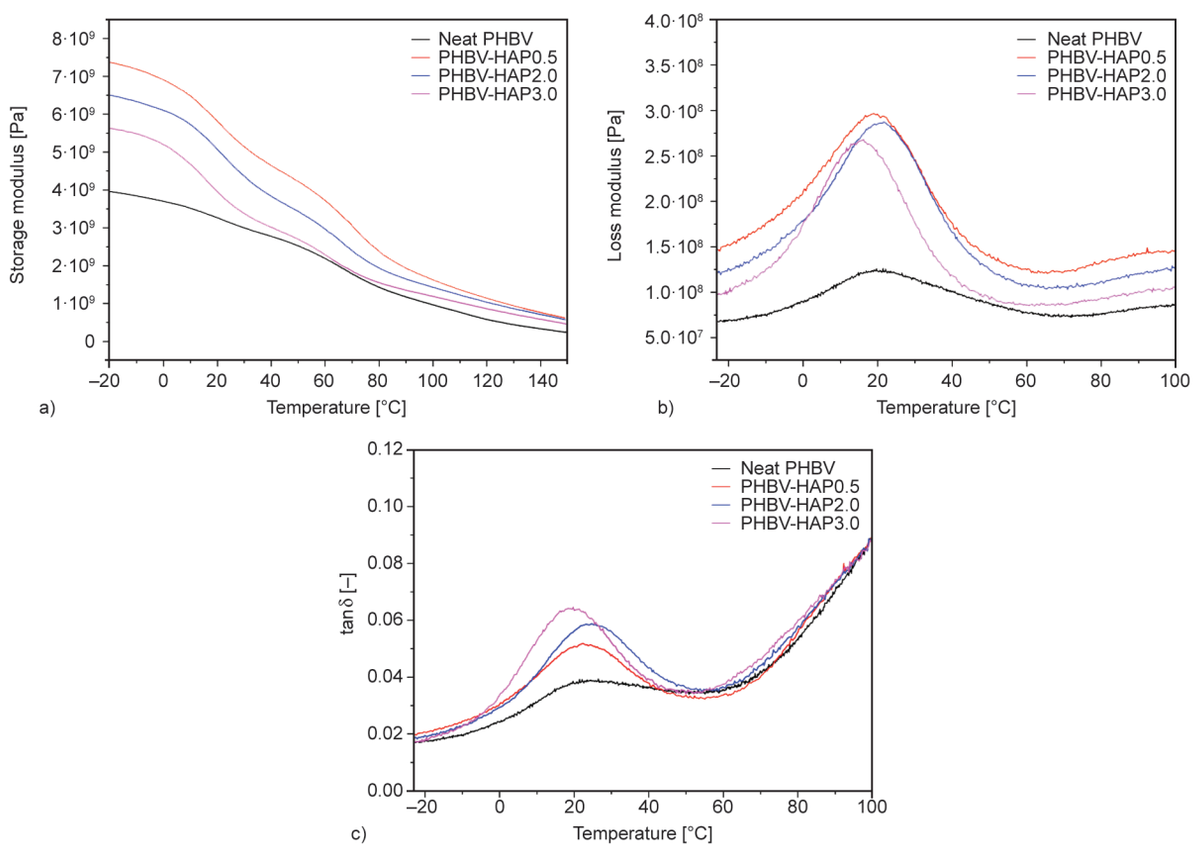

Figure 6. DMA thermographs for PHBV-SiHAP bionanocomposites show a) storage modulus, b) loss modulus, and c) tan δ.

E''. However, the loss modulus drops above glass transition temperature (T_g) since less force is needed to cause deformation.

Dynamic mechanical analysis is a valuable tool to determine the material's glass transition temperature, typically taken as the peak of the tan δ curve generated through a temperature ramp experiment. Figure 6c shows the temperature-dependent loss tangent (tan δ) values for the PHBV and composite materials. In viscoelastic materials, internal friction is represented by the loss tangent (tan δ), which is the ratio of the loss modulus (E'') to the storage modulus (E'). It is an assessment of energy wasted that is expressed in terms of energy recovered. The values of relaxation temperatures connected to the glass transition temperature were taken at the maximum of the peak of the damping factor.

The neat and PHBV composites' glass transition region is between 22–26 °C. The tan δ curve of the composites (Figure 6c) showed that the T_g values decreased with the increase in filler loading. T_g of neat PHBV decreases from 26 to 19 °C by incorporating 3 wt% SiHAP.

Srithep *et al.* [53] prepared poly(3-hydroxybutyrate-*co*-3-hydroxyvalerate, PHBV) and nanofibrillated cellulose (NFC) nanocomposites by melt compounding. Compared to neat PHBV at 25 °C, the storage modulus for nanocomposite reinforced with 10 wt% NFC increased by 28%. The composite's glass transition temperature slightly increased with increasing NFC. On the other hand, the relaxation process strongly decreased with increasing NFC, which was attributed to the limitation of chain mobility within the polymer matrix. Chen and Wang [54] investigated PHBV/HAP and PHBV/tricalcium phosphate (TCP) biocomposites. The elastic modulus of PHBV at 30% particle loading is reinforced by 21.26 wt% (TCP) and 37.17 wt% of HAP at 37 °C. The addition of bioceramic particles generally reduced tan δ for both PHBV/HAP and PHBV/TCP composites [54]. PHBV nanocomposites were fabricated by incorporating nano-sized hydroxyapatite (nHAP) by a solution casting method [32]. The storage modulus of the PHBV/HAP (100/30) nanocomposite was increased by 41.2% at –50 °C and 99.1% at 75 °C at 1 Hz. The neat and PHBV composites glass transition temperature region was found between 17.1–17.6 °C at 1 Hz [32]. PHBV and purified alpha-cellulose fibers were prepared by melt blending. No noticeable changes in T_g values of the composites were found for low cellulose content with respect to the neat PHBV [55]. PLA nanocomposites were prepared using surface-treated (mNHAP) and untreated nanohydroxyapatite (mNHAP) [56]. Nanocomposites prepared with surface-treated nanohydroxyapatite showed a significant decrease in T_g. They concluded that reduced glass transition temperature is a measure of poor interfacial adhesion between the PLA matrix and mNHAP [56]. Mittal *et al.* [57] investigated the effect of talc and mica particles on the properties of polypropylene. It was found that when talc and mica loading increased, tan delta values decreased. This result was explained by the disruption of the polymer chain packing due to the filling up of the free volume of the polymer by talc and mica particles [57]. PHBV, nanodiamond (nD), and nanohydroxyapatite (nHAP) loaded with vancomycin (VC) nanocomposites were prepared using a rotary evaporator (PHBV/nHAP/VC/nD-R) or spray drying (PHBV/nHAP/VC/nD-SD) [48]. The storage modulus of the composites prepared by the rotary evaporator increased by 51.7% at 37 °C, but T_g value decreased from 17 to 14.8 °C for neat polymer and composite, respectively. This result was explained by the agglomeration of nanoparticles. Since nano HAP particles have the propensity to aggregate, particularly at high concentrations, the same argument can be taken into account in this work.

3.6. Screening of cytotoxicity

Biocompatibility is one of the most significant features of biomaterials that are preferred used in tissue engineering applications. Biomaterials are expected to improve cell attachment, proliferation, and migration. Furthermore, tissue scaffolds should not demonstrate cytotoxicity and prevent the generation of toxic byproducts during degradation [58]. So, within the context of the present study, we explored the possible interactions between osteoblast cells and synthesized composites with variable compositions to understand their probable utilities for biomedical applications. For biological activity experiments, we primarily examined the cytotoxicity of prepared composites.

To evaluate the cellular viability rates of osteoblasts that were treated with neat PHBV and their composites derived with the addition of different values of Si-doped HAP, the MTT method was used. Biocomposites were extracted within a culture medium for 48 hours, and extracts were applied on SaOs-2

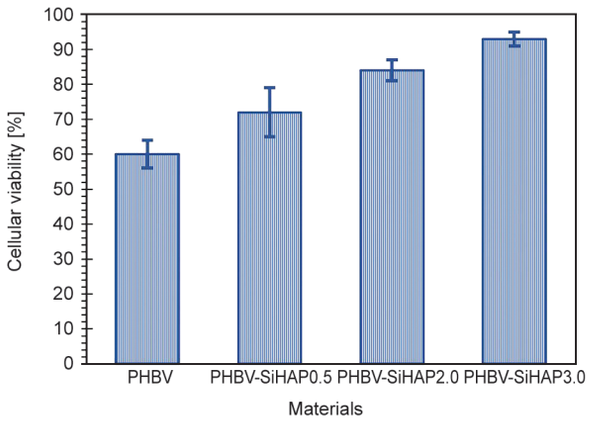

Figure 7. Cellular viability rates of osteoblast cells that were exposed to different biomaterials for 96 hours.

osteoblast cells for 96 hours before measurement of cellular viability degrees. Figure 7 indicates the cellular viability ratios of osteoblast cells after treatment with extracts. As it is seen in Figure 7, neat PHBV leads to a reduction in viability rates. It was detected that PHBV treatment declined cellular viability at 40%. Only 60% of cells were alive after their exposure to PHBV. On the other side, it was also examined from Figure 7 that the addition of SiHAP into PHBV positively impacts their biocompatibilities since cell vitalities are significantly augmented in contrast to using PHBV alone. Interestingly, it was discovered that there were proportional increases in the numbers of cells according to increasing SiHAP within the composites. The highest cellular viability ratio was measured in the group prepared with 3 wt% SiHAP. Approximately 92% cellular viability was measured in the mentioned group. In contrast, to control, the ratio of viable cells was counted as 72 and 84% in experimental groups prepared by 0.5 and 2 wt% SiHAP, respectively. These results revealed that the toxic feature of PHBV could be reversed by adding SiHAP with enhanced dosages. Numerous studies detected that bioactivity and biocompatibility features of PHBV scaffolds improved remarkably when they were incorporated with other polymers to generate composites. For instance, Degli Esposti, *et al.* [59] synthesized several scaffolds, including PHBV, PHBV-hydroxyapatite, PHBV-calcium silicate, PHBV-bioglass to investigate their possible use for bone tissue engineering. In cytotoxicity assay, researchers determined that the use of a PHBV scaffold decreased cellular viability rates of fibroblast cells to 60%. It was also revealed that the use of combinations of PHBV with bioactive inorganic particles enhanced cellular viabilities significantly, in contrast to the use of PHBV scaffold alone [59]. In another study, Wu *et al.* [60] discovered that PHBV-bioglass composite scaffolds were more effective in terms of vascularization stimulation for bone tissue recovery when compared with the use of PHBV scaffold. In the scope of mentioned articles, the results of the current study indicate that the PHBV scaffold declined the cell viability rates. At the same time, composites possessed better biocompatibility is consistent with the previous research.

3.7. DAPI staining for determination of biocompatibility

The biocompatibility features of synthesized nanobiomaterials were also explored by visualizing the attachment of cells onto variable composites. The amounts of cells adhered to biomaterials were monitored by DAPI staining. Figure 8 represents the microscopic views indicating the changes in the amounts of fibroblast cells adhered to biocomposites. As observed, the numbers of attached cells onto samples were at the lowest degree in the group where we used neat PHBV, suggesting that this biomaterial possessed low biocompatibility. In contrast, the numbers of attached cells on samples remarkably lifted when PHBV composites were prepared with different concentrations of SiHAP. The highest biocompatibility property was detected in the group in which the composite was prepared with SiHAP at a 3 wt% concentration. When mentioned biocomposite was applied, the numbers of attached cells on the composite were seen at the highest level. These data showed that the biocompatibility feature of PHBV improved by adding SiHAP at enhanced concentrations. These results are also coherent with the data from cytotoxicity experiments. Both results decipher that composites prepared by PHBV and SiHAP could advance cells' proliferation and migration abilities while massively reducing the toxicity originating from PHBV. Obtained results are also coherent with the data acquired from previous articles. In a similar study, Huang *et al.* [61] conjugated HAP nanoplates with polylactide polymer and investigated the bioavailability of newly synthesized nanocomposites for bone tissue engineering. Authors exhibited that cell proliferation rates of murine preosteoblast cell line (MC3T3-E1) osteoblast cells decreased to 60% at the end of 24 h incubation when polylactide polymer was applied alone. On the other side, adding HAP nanoparticles into the polymeric material enormously

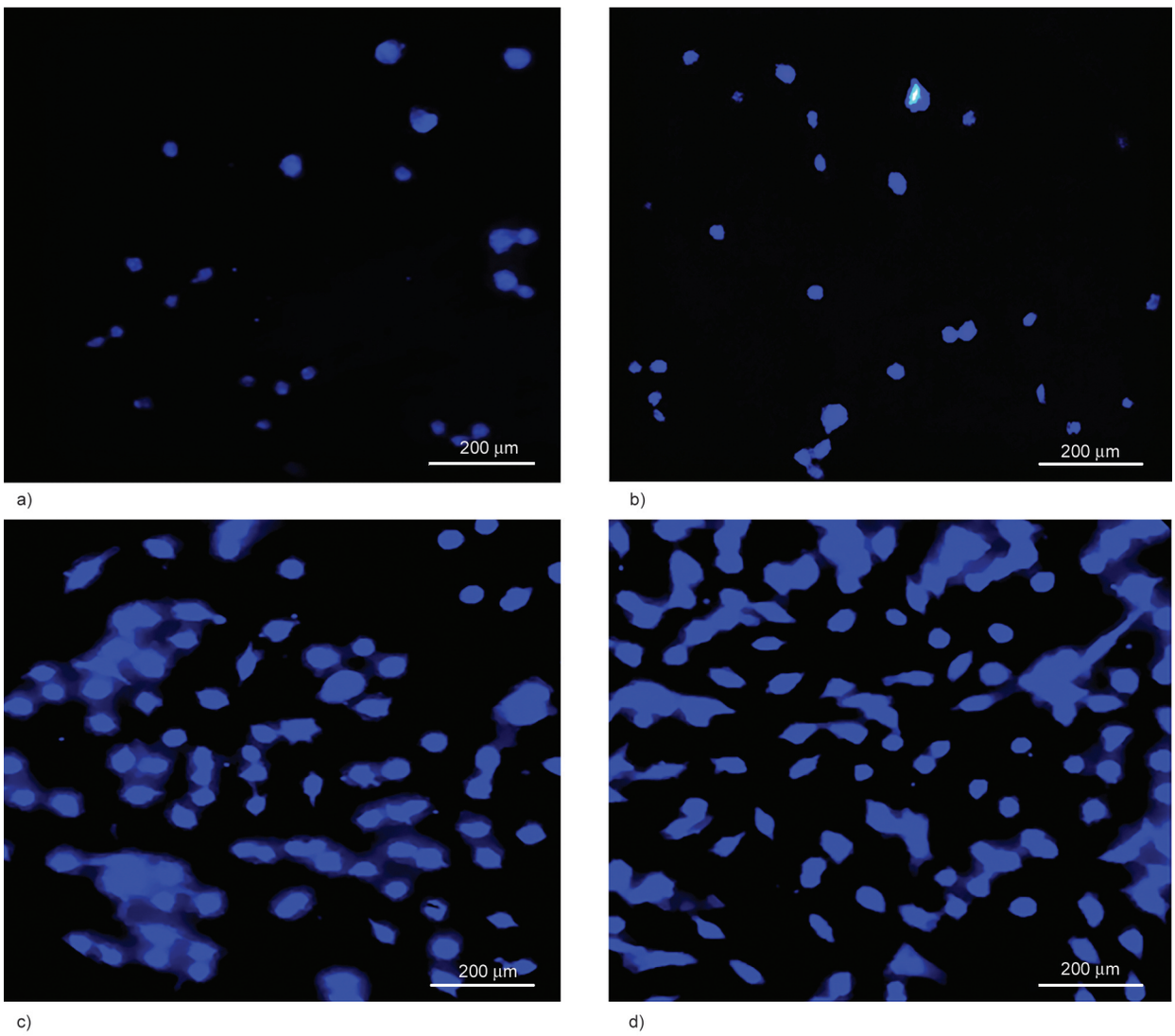

Figure 8. Morphological views of fibroblast cells that were seeded onto a) PHBV, b) PHBV-SiHAP0.5, c) PHBV-SiHAP 2.0, d) PHBV-SiHAP 3.0.

lifted the cellular vitality degrees of osteoblasts following 24 h incubation. Additionally, high osteoblast viability was evaluated in response to the scaffold application, including increased nano-HAP concentrations. At all investigated time intervals, the numbers of osteoblasts were higher in the group in which they were exposed to composites in comparison to the use of polymer alone. In another experiment, researchers accounted for the cell spreading over tested scaffolds. Results showed that approximately 2 mm of scaffolds were covered with osteoblasts in the group in which the composite included 15% HAP. Moreover, it was also determined that the numbers of cells that were adhered to scaffolds were lower in the group in which polylactide was used alone in contrast to the application of polymers incorporated with nano-HAP, according to fluorescence microscopy results. Suslu *et al.* [7] prepared HAP-PHBV nanofibers as a biocomposite by electrospinning technique in another research similar to ours. They exhibited that these nanofibers, including HAP, synthesized with different surfactants, extensively ameliorated the osteoconductive feature of the PHBV scaffold.

Bioactivity and biocompatibility features of SiHAP were proven in previous studies. In one of them, Sun *et al.* [19] combined HAP and silicone to prepare scaffolds for bone tissue engineering and examined the bioactivity of prepared composites. Outputs showed that adding silicone at various dosages did not influence the cytocompatibility properties of HAP, and both HAP and HAP-silicone composites were found biocompatible at variable concentrations ranging between 25 and 400 µg/ml.

This study is the first report indicating that PHBV-SiHAP composites enhance cell proliferation and

migration while decreasing the cytotoxicity of PHBV. In light of this research, we proposed that SiHAP-enriched PHBV could be a promising alternative for using biomedical applications.

4. Conclusions

PHBV reinforced with SiHAP nanocrystals was successfully obtained by melt extrusion using different amounts of particles (0.5, 2, and 3 wt%). We assessed the physical, thermal, thermomechanical, and biological properties of the PHBV-SiHAP bionanocomposites. SiHAP nanoparticles increased the crystallinity of the PHBV matrix, which was confirmed by the XRD analysis. All nanocomposites exhibited improved storage modulus with the addition of SiHAP. The storage modulus of PHBV increases by 80% for PHBV-SiHAP0.5 HAP at 20 °C. This result may be related to the favorable interactions between the polymer matrix and SiHAP that restrict the movement of polymer chains. All these results showed that Si-doped HAP is a very effective reinforcing agent reaching a higher storage modulus with a considerably lower fraction.

We found that the neat PHBV was not tolerable in terms of toxicity since cellular viability rates were assessed as 60% after using sample extracts. However, it was ascertained that adding SiHAP at enhanced concentrations led to noticeable improvements in cellular viability ratios. It was detected that cell viability rates reached 92% when composite including PHBV and SiHAP 3 wt% were performed. These data elicit absolute compatibility between high cell viability rates and advanced SiHAP concentrations. It can be concluded that enrichment of PHBV with increased SiHAP dosages could improve the bioavailability of polymer.

DAPI staining experiments reflected that PHBV-SiHAP composites ensured significant increases in cell attachment, proliferation, and migration in comparison to PHBV polymeric scaffold. In addition, we also established that proliferation and migration levels of osteoblasts markedly augmented as a response to advances in the concentrations of SiHAP within the composites under fluorescence microscope images.

Obtained results in the present study reveal that SiHAP reinforced PHBV composites were completely bioavailable and biocompatible. We suggest that these novel composites that meet the mechanical strength, bioactive, biocompatible, and non-toxic requirements of biomaterials are promising biocomposites for biomedical applications.

Acknowledgements

This research has been supported by the Research Fund of the Yıldız Technical University. Project Number: FYL-2021-4650.

References

[1] Pantani R., Turng L-S.: Manufacturing of advanced biodegradable polymeric components. Journal of Applied Polymer Science, **132**, 42889 (2015). https://doi.org/10.1002/app.42889

[2] Silva A. P. B., Montagna L. S., Passador F. R., Rezende M. C., Lemes A. P.: Biodegradable nanocomposites based on PLA/PHBV blend reinforced with carbon nanotubes with potential for electrical and electromagnetic applications. Express Polymer Letters, **15**, 987–1003 (2021). https://doi.org/10.3144/expresspolymlett.2021.79

[3] Jost V.: Packaging related properties of commercially available biopolymers – An overview of the status quo. Express Polymer Letters, **12**, 429–435 (2018). https://doi.org/10.3144/expresspolymlett.2018.36

[4] Khardenavis A. A., Suresh Kumar M., Mudliar S. N., Chakrabarti T.: Biotechnological conversion of agro-industrial wastewaters into biodegradable plastic, poly β-hydroxybutyrate. Bioresource Technology, **98**, 3579–3584 (2007). https://doi.org/10.1016/j.biortech.2006.11.024

[5] Lenz R. W., Marchessault R. H.: Bacterial polyesters: Biosynthesis, biodegradable plastics and biotechnology. Biomacromolecules, **6**, 1–8 (2005). https://doi.org/10.1021/bm049700c

[6] Sadat-Shojai M.: Electrospun polyhydroxybutyrate/hydroxyapatite nanohybrids: Microstructure and bone cell response. Journal of Materials Science and Technology, **32**, 1013–1020 (2016). https://doi.org/10.1016/j.jmst.2016.07.007

[7] Suslu A., Albayrak A. Z., Urkmez A. S., Bayir E., Cocen U.: Effect of surfactant types on the biocompatibility of electrospun HAp/PHBV composite nanofibers. Journal of Materials Science: Materials in Medicine, **25**, 2677–2689 (2014). https://doi.org/10.1007/s10856-014-5286-1

[8] Sadat-Shojai M., Khorasani M-T., Jamshidi A., Irani S.: Nano-hydroxyapatite reinforced polyhydroxybutyrate composites: A comprehensive study on the structural and *in vitro* biological properties. Materials Science and Engineering C, **33**, 2776–2787 (2013). https://doi.org/10.1016/j.msec.2013.02.041

[9] Panayotidou E., Kroustalli A., Baklavaridis A., Zuburtikudis I., Achilias D. S., Deligianni D.: Biopolyester-based nanocomposites: Structural, thermo-mechanical and biocompatibility characteristics of poly(3-hydroxybutyrate)/montmorillonite clay nanohybrids. Journal of Applied Polymer Science, **132**, 41628 (2015). https://doi.org/10.1002/app.41628

[10] Anjum A., Zuber M., Zia K. M., Noreen A., Anjum M. N., Tabasum S.: Microbial production of polyhydroxyalkanoates (PHAs) and its copolymers: A review of recent advancements. International Journal of Biological Macromolecules, **89**, 161–174 (2016). https://doi.org/10.1016/j.ijbiomac.2016.04.069

[11] Knowles J. C., Hastings G. W., Ohta H., Niwa S., Boeree N.: Development of a degradable composite for orthopaedic use: *In vivo* biomechanical and histological evaluation of two bioactive degradable composites based on the polyhydroxybutyrate polymer. Biometarials, **13**, 491–496 (1992). https://doi.org/10.1016/0142-9612(92)90099-A

[12] Luzier W. D.: Materials derived from biomass/biodegradable materials. PNAS, **89**, 839–842 (1992). https://doi.org/10.1073/pnas.89.3.839

[13] Wang N., Zhou Z., Xia L., Dai Y., Liu H.: Fabrication and characterization of bioactive β-Ca_2SiO_4/PHBV composite scaffolds. Materials Science and Engineering C, **33**, 2294–2301 (2013). https://doi.org/10.1016/j.msec.2013.01.059

[14] Sultana N., Khan T. H.: *In vitro* degradation of PHBV scaffolds and nHA/PHBV composite scaffolds containing hydroxyapatite nanoparticles for bone tissue engineering. Journal of Nanomaterials, **2012**, 190950 (2012). https://doi.org/10.1155/2012/190950

[15] Gogolewski S., Jovanovic M., Perren S. M., Dillon J. G., Hughes' M. K.: Tissue response and *in vivo* degradation of selected polyhydroxyacids: Polylactides (PLA), poly(3-hydroxybutyrate) (PHB), and poly(3-hydroxybutyrate-*co*-3-hydroxyvalerate) (PHB/VA). Journal of Biomedical Materials Research, **27**, 1135–1147 (1993). https://doi.org/10.1002/jbm.820270904

[16] Bassett D. C.: Developments in crystalline polymers. Springer, Dordrecht (1988). https://doi.org/10.1007/978-94-009-1341-7

[17] Liu J., Zhao B., Zhang Y., Lin Y., Hu P., Ye C.: PHBV and predifferentiated human adipose-derived stem cells for cartilage tissue engineering. Journal of Biomedical Materials Research: Part A, **94**, 603–610 (2010). https://doi.org/10.1002/jbm.a.32730

[18] Alizadeh-Osgouei M., Li Y., Wen C.: A comprehensive review of biodegradable synthetic polymer-ceramic composites and their manufacture for biomedical applications. Bioactive Materials, **4**, 22–36 (2019). https://doi.org/10.1016/j.bioactmat.2018.11.003

[19] Sun T., Wang M., Shao Y., Wang L., Zhu Y.: The effect and osteoblast signaling response of trace silicon doping hydroxyapatite. Biological Trace Element Research, **181**, 82–94 (2018). https://doi.org/10.1007/s12011-017-1031-1

[20] Qiao H., Song G., Huang Y., Yang H., Han S., Zhang X., Wang Z., Ma J., Bu X., Fu L.: Si, Sr, Ag *co*-doped hydroxyapatite/TiO_2 coating: Enhancement of its antibacterial activity and osteoinductivity. RSC Advances, **9**, 13348–13364 (2019). https://doi.org/10.1039/c9ra01168d

[21] Arcos D., Rodríguez-Carvajal J., Vallet-Regí M.: Silicon incorporation in hydroxylapatite obtained by controlled crystallization. Chemistry of Materials, **16**, 2300–2308 (2004). https://doi.org/10.1021/cm035337p

[22] Botelho C. M., Brooks R. A., Best S. M., Lopes M. A., Santos J. D., Rushton N., Bonfield W.: Human osteoblast response to silicon-substituted hydroxyapatite. Journal of Biomedical Materials Research: Part A, **79**, 723–730 (2006). https://doi.org/10.1002/jbm.a.30806

[23] Balamurugan A., Rebelo A. H. S., Lemos A. F., Rocha J. H. G., Ventura J. M. G., Ferreira J. M. F.: Suitability evaluation of sol-gel derived Si-substituted hydroxyapatite for dental and maxillofacial applications through *in vitro* osteoblasts response. Dental Materials, **24**, 1374–1380 (2008). https://doi.org/10.1016/j.dental.2008.02.017

[24] Gomes P. S., Botelho C., Lopes M. A., Santos J. D., Fernandes M. H.: Evaluation of human osteoblastic cell response to plasma-sprayed silicon-substituted hydroxyapatite coatings over titanium substrates. Journal of Biomedical Materials Research Part B: Applied Biomaterials, **94**, 337–346 (2010). https://doi.org/10.1002/jbm.b.31656

[25] Balas F., Pérez-Pariente J., Vallet-Regí M.: *In vitro* bioactivity of silicon-substituted hydroxyapatites. Journal of Biomedical Materials Research, **A66**, 364–375 (2003). https://doi.org/10.1002/jbm.a.10579

[26] Russias J., Saiz E., Nalla R. K., Gryn K., Ritchie R. O., Tomsia A. P.: Fabrication and mechanical properties of PLA/HA composites: A study of *in vitro* degradation. Materials Science and Engineering C, **26**, 1289–1295 (2006). https://doi.org/10.1016/j.msec.2005.08.004

[27] Ignjatovic N., Uskokovic D.: Synthesis and application of hydroxyapatite/polylactide composite biomaterial. Applied Surface Science, **238**, 314–319 (2004). https://doi.org/10.1016/j.apsusc.2004.05.227

[28] Freier T.: Biopolyesters in tissue engineering applications. Advances in Polymer Science **203**, 1–61 (2006). https://doi.org/10.1007/12_073

[29] Shishatskaya E. I., Khlusov I. A., Volova T. G.: A hybrid PHB–hydroxyapatite composite for biomedical application: Production, *in vitro* and *in vivo* investigation. Journal of Biomaterials Science, Polymer Edition, **17**, 481–498 (2006). https://doi.org/10.1163/156856206776986242

[30] Nahanmoghadam A., Asemani M., Goodarzi V., Ebrahimi-Barough S.: *In vivo* investigation of PCL/PHBV/hydroxyapatite nanocomposite scaffold in regeneration of critical-sized bone defects. Fibers and Polymers, **22**, 2507–2516 (2021). https://doi.org/10.1007/s12221-021-1243-z

[31] Yuan J., Zheng Q., Cheng J.: Fabrication, characterization and adsorptive of human fibrinogen of HA/PHBV nanocomposite films. Advanced Materials Research, **160–162**, 1325–1330 (2011). https://doi.org/10.4028/www.scientific.net/AMR.160-162.1325

[32] Chen D. Z., Tang C. Y., Chan K. C., Tsui C. P., Yu P. H. F., Leung M. C. P., Uskokovic P. S.: Dynamic mechanical properties and *in vitro* bioactivity of PHBHV/HA nanocomposite. Composites Science and Technology, **67**, 1617–1626 (2007). https://doi.org/10.1016/j.compscitech.2006.07.034

[33] Rai B., Noohom W., Kithva P. H., Grøndahl L., Trau M.: Bionanohydroxyapatite/poly(3-hydroxybutyrate-*co*-3-hydroxyvalerate) composites with improved particle dispersion and superior mechanical properties. Chemistry of Materials, **20**, 2802–2808 (2008). https://doi.org/10.1021/cm703045u

[34] Öner M., İlhan B.: Fabrication of poly(3-hydroxybutyrate-*co*-3-hydroxyvalerate) biocomposites with reinforcement by hydroxyapatite using extrusion processing. Materials Science and Engineering C, **65**, 19–26 (2016). https://doi.org/10.1016/j.msec.2016.04.024

[35] Yu H., Sun B., Zhang D., Chen G., Yang X., Yao J.: Reinforcement of biodegradable poly(3-hydroxybutyrate-*co*-3-hydroxyvalerate) with cellulose nanocrystal/silver nanohybrids as bifunctional nanofillers. Journal of Materials Chemistry B, **2**, 8479–8489 (2014). https://doi.org/10.1039/c4tb01372g

[36] Huang W., Wang Y., Ren L., Du C., Shi X.: A novel PHBV/HA microsphere releasing system loaded with alendronate. Materials Science and Engineering C, **29**, 2221–2225 (2009). https://doi.org/10.1016/j.msec.2009.05.015

[37] Kawamura Y., Gan H., Kabe T., Maehara A., Kimura S., Hikima T., Takata M., Iwata T.: Mechanism of elastic properties of biodegradable poly[(R)-3-hydroxybutyrate-*co*-4-hydroxybutyrate] films revealed by synchrotron radiation. ACS Omega, **6**, 7387–7393 (2021). https://doi.org/10.1021/acsomega.0c05662

[38] Zhijiang C., Guang Y.: Optical nanocomposites prepared by incorporating bacterial cellulose nanofibrils into poly(3-hydroxybutyrate). Materials Letters, **65**, 182–184 (2011). https://doi.org/10.1016/j.matlet.2010.09.055

[39] Öner M., Kızıl G., Keskin G., Pochat-Bohatier C., Bechelany M.: The effect of boron nitride on the thermal and mechanical properties of poly(3-hydroxybutyrate-*co*-3-hydroxyvalerate). Nanomaterials, **8**, 940 (2018). https://doi.org/10.3390/nano8110940

[40] Rusmirović J. D., Ivanović J. Z., Pavlović V. B., Rakić V. M., Rančić M. P., Djokić V., Marinković A. D.: Novel modified nanocellulose applicable as reinforcement in high-performance nanocomposites. Carbohydrate Polymers, **164**, 64–74 (2017). https://doi.org/10.1016/j.carbpol.2017.01.086

[41] Ambrosio-Martín J., Gorrasi G., Lopez-Rubio A., Fabra M. J., Mas L. C., Lõpez-Manchado M. A., Lagaron J. M.: On the use of ball milling to develop poly(3-hydroxybutyrate-*co*-3-hydroxyvalerate)-graphene nanocomposites (II) – Mechanical, barrier, and electrical properties. Journal of Applied Polymer Science, **132**, 42217 (2015). https://doi.org/10.1002/app.42217

[42] Yu H., Yan C., Yao J.: Fully biodegradable food packaging materials based on functionalized cellulose nanocrystals/poly(3-hydroxybutyrate-*co*-3-hydroxyvalerate) nanocomposites. RSC Advances, **4**, 59792–59802 (2014). https://doi.org/10.1039/c4ra12691b

[43] Wei L., McDonald A. G., Stark N. M.: Grafting of bacterial polyhydroxybutyrate (PHB) onto cellulose *via in situ* reactive extrusion with dicumyl peroxide. Biomacromolecules, **16**, 1040–1049 (2015). https://doi.org/10.1021/acs.biomac.5b00049

[44] Díez-Pascual A. M., Díez-Vicente A. L.: ZnO-reinforced poly(3-hydroxybutyrate-*co*-3-hydroxyvalerate) bionanocomposites with antimicrobial function for food packaging. ACS Applied Materials and Interfaces, **6**, 9822–9834 (2014). https://doi.org/10.1021/am502261e

[45] Lemes A. P., Soto-Oviedo M. A., Waldman W. R., Innocentini-Mei L. H., Durán N.: Effect of lignosulfonate on the thermal and morphological behavior of poly(3-hydroxybutyrate-*co*-3-hydroxyvalerate). Journal of Polymers and the Environment, **18**, 250–259 (2010). https://doi.org/10.1007/s10924-010-0170-7

[46] Ten E., Turtle J., Bahr D., Jiang L., Wolcott M.: Thermal and mechanical properties of poly(3-hydroxybutyrate-*co*-3-hydroxyvalerate)/cellulose nanowhiskers composites. Polymer, **51**, 2652–2660 (2010). https://doi.org/10.1016/j.polymer.2010.04.007

[47] Wang S., Xiang H., Wang R., Zhou Z., Zhu M.: Influence of amorphous alkaline lignin on the crystallization behavior and thermal properties of bacterial polyester. Journal of Applied Polymer Science, **132**, 41325 (2015). https://doi.org/10.1002/app.41325

[48] de Almeida Neto G. R., Barcelos M. V., Ribeiro M. E. A., Folly M. M., Rodríguez R. J. S.: Formulation and characterization of a novel PHBV nanocomposite for bone defect filling and infection treatment. Materials Science and Engineering C, **104**, 110004 (2019). https://doi.org/10.1016/j.msec.2019.110004

[49] Ambrosio-Martín J., Gorrasi G., Lopez-Rubio A., Fabra M. J., Mas L. C., Lõpez-Manchado M. A., Lagaron J. M.: On the use of ball milling to develop PHBV–graphene nanocomposites (I) – Morphology, thermal properties, and thermal stability. Journal of Applied Polymer Science, **132**, 42101 (2015). https://doi.org/10.1002/app.42101

[50] Castro-Mayorga J. L., Fabra M. J., Pourrahimi A. M., Olsson R. T., Lagaron J. M.: The impact of zinc oxide particle morphology as an antimicrobial and when incorporated in poly(3-hydroxybutyrate-*co*-3-hydroxyvalerate) films for food packaging and food contact surfaces applications. Food and Bioproducts Processing, **101**, 32–44 (2017). https://doi.org/10.1016/j.fbp.2016.10.007

[51] Anžlovar A., Kržan A., Žagar E.: Degradation of PLA/ZnO and PHBV/ZnO composites prepared by melt processing. Arabian Journal of Chemistry, **11**, 343–352 (2018). https://doi.org/10.1016/j.arabjc.2017.07.001

[52] Braga N. F., Vital D. A., Guerrini L. M., Lemes A. P., Formaggio D. M. D., Tada D. B., Arantes T. M., Cristovan F. H.: PHBV-TiO_2 mats prepared by electrospinning technique: Physico-chemical properties and cytocompatibility. Biopolymers, **109**, e23120 (2018). https://doi.org/10.1002/bip.23120

[53] Srithep Y., Ellingham T., Peng J., Sabo R., Clemons C., Turng L-S., Pilla S.: Melt compounding of poly(3-hydroxybutyrate-*co*-3-hydroxyvalerate)/nanofibrillated cellulose nanocomposites. Polymer Degradation and Stability, **98**, 1439–1449 (2013). https://doi.org/10.1016/j.polymdegradstab.2013.05.006

[54] Chen L. J., Wang M.: Production and evaluation of biodegradable composites based on PHB-PHV copolymer. Biomaterials, **23**, 2631–2639 (2002). https://doi.org/10.1016/S0142-9612(01)00394-5

[55] Sánchez-Safont E. L., González-Ausejo J., Gámez-Pérez J., Lagarón J. M., Cabedo L.: Poly(3-hydroxybutyrate-*co*-3-hydroxyvalerate)/ purified cellulose fiber composites by melt blending: Characterization and degradation in composting conditions. Journal of Renewable Materials, **4**, 123–132 (2016). https://doi.org/10.7569/JRM.2015.634127

[56] Michael F. M., Khalid M., Raju G., Ratnam C. T., Walvekar R., Mubarak N. M.: Viscoelastic properties and thermal stability of nanohydroxyapatite reinforced poly(lactic acid) for load bearing applications. Molecules, **26**, 5852 (2021). https://doi.org/10.3390/molecules26195852

[57] Mittal P., Naresh S., Luthra P., Singh A., Dhaliwal J. S., Kapur G. S.: Polypropylene composites reinforced with hybrid inorganic fillers: Morphological, mechanical, and rheological properties. Journal of Thermoplastic Composite Materials, **32**, 848–864 (2019). https://doi.org/10.1177/0892705718785674

[58] Jack K. S., Velayudhan S., Luckman P., Trau M., Grøndahl L., Cooper-White J.: The fabrication and characterization of biodegradable HA/PHBV nanoparticle-polymer composite scaffolds. Acta Biomaterialia, **5**, 2657–2667 (2009). https://doi.org/10.1016/j.actbio.2009.03.017

[59] Esposti M. D., Changizi M., Salvatori R., Chiarini L., Cannillo V., Morselli D., Fabbri P.: Comparative study on bioactive filler/biopolymer scaffolds for potential application in supporting bone tissue regeneration. ACS Applied Polymer Materials, **4**, 4306–4318 (2022). https://doi.org/10.1021/acsapm.2c00270

[60] Wu J., Wu Z., Xue Z., Li H., Liu J.: PHBV/bioglass composite scaffolds with co-cultures of endothelial cells and bone marrow stromal cells improve vascularization and osteogenesis for bone tissue engineering. RSC Advances, **7**, 22197–22207 (2017). https://doi.org/10.1039/c7ra02767b

[61] Huang Z., Wan Y., Peng M., Yang Z., Luo H.: Incorporating nanoplate-like hydroxyapatite into polylactide for biomimetic nanocomposites *via* direct melt intercalation. Composites Science and Technology, **185**, 107903 (2020). https://doi.org/10.1016/j.compscitech.2019.107903